Supporting Information for "Rapid viscoelastic deformation slows marine ice sheet instability at Pine Island Glacier"

S. B. Kachuck[1]*, D. F. Martin[2], J. N. Bassis[1], and S. Price[3]

[1]Climate and Space Sciences and Engineering, University of Michigan, Ann Arbor, MI, USA

[2]Applied Numerical Algorithms Group, Lawrence Berkeley National Laboratory, Berkeley, CA, USA

[3]Fluid Dynamics and Solid Mechanics Group, Los Alamos National Laboratory, P.O. Box 1663, MS B216, Los Alamos, NM 87545, USA

Contents of this file

1. Text S1. GIA-deformation model
2. Text S2. Committed uplift
3. Figure S1. Viscoelastic Mode Comparisons
4. Figure S2. Elastic effects
5. Figure S3. Estimated geoid effects
6. Figure S4. Estimated committed uplift
7. Figure S5. Additional simulation runs

Introduction

This supporting information contains additional details for the GIA model used in this study. Texts S1 and S2 describe details of the GIA coupling and a method for estimating the committed uplift remaining at the start of the simulation. Figure S1 compares methods of approximating the viscoelastic response of the Earth, showing that the dominant modes of all three methods agree for small wavelengths. Figures S2-S4 show the effect on ice dynamics of additional components of the solid-earth response: instantaneous elastic deformation, perturbations to the geoid, and committed uplift, respectively. Figure S5 summarizes the effect on ice mass loss of changing other assumptions.

1. Text S1. GIA-deformation model

We use an adaptation of the 2D FFT-based GIA model of Bueler, Lingle, and Kallen-Brown (2007) for two- and three-layer mantles, briefly described here. The model is an improvement over elastic lithosphere, relaxing asthenosphere (ELRA) models (e.g., Le Muir & Huybrechts, 1996 and Huybrechts, 2002), which use only one decay constant for the viscous relaxation of the underlying mantle, because long- and short-wavelength loads relax quickly by engaging more of the mantle in its relaxation and by being supported elastically by the lithosphere, respectively. The Bueler et al. (2007) spectral collocation method updates the Fourier transformed uplift field $\hat{U}_{\mathbf{k}}$ (with wavevector $\mathbf{k}$) at each step using the previously computed uplift and a Fourier transformed load $\hat{L}_{\mathbf{k}}$ computed halfway between the two using

$$\hat{U}_{\mathbf{k}}^{n+1} = \frac{(\tau - \frac{1}{2}\Delta t)\hat{U}_{\mathbf{k}}^{n} + T\Delta t(\hat{L}_{\mathbf{k}}^{n+1})}{(\tau + \frac{1}{2}\Delta t)}, \tag{1}$$

where we have recast their original formula (11) in terms of the transfer function T (units m / Pa) which relates a load to the deformation at equilibrium (substituting $\hat{U}_{\mathbf{k}}^{n+1} = \hat{U}_{\mathbf{k}}^{n} = \hat{U}_{\mathbf{k}}^{\mathrm{eq}}$ into the above we find $\hat{U}_{\mathbf{k}}^{\mathrm{eq}} = T\hat{L}_{\mathbf{k}}$), and a decay constant τ.

For the two-layer, incompressible, viscous halfspace overlain by an infinitesimal elastic sheet described by Bueler et al. (2007), the transfer function is given by

$$T = (\rho_r g + |\mathbf{k}|^4 D)^{-1}, \tag{2}$$

for a mantle of density ρ_r and constant gravity g. This is equivalent to the inverse of their factor β. The first term in equation 2 is the amount of deformation of a fluid in hydrostatic equilibrium (or complete isostatic compensation). The second term arises from the finite support of the load due to elastic stresses in the lithosphere, and therefore a reduction of the possible compensation by buoyancy. The term is related to the flexural rigidity D of the lithosphere, which depends on the thickness of the plate h_e by

$$D = \frac{E h_e^3}{12(1-\nu^2)}, \tag{3}$$

for a lithosphere with Young's modulus E and Poisson's ratio ν. This T is shown as a function of wavelength in figure S1(b) for a lithosphere with effective elastic thicknesses of 25 km (solid). An order of magnitude increase in flexural rigidity (a little over doubling the thickness) results in elastic stresses that support 90% more of small-wavelength loads, which thus decreases the total viscous deformation by an order of magnitude. Note that T goes to zero for large k, showing that the lithosphere limits the magnitude of the viscoelastic compensation of small wavelength (large wavenumber) loads, analogous to a low-pass filter for loads.

The time constant τ for the one- and two-layer viscous models is given by

$$\tau = 2T\eta_1|\mathbf{k}|\mathcal{R} \tag{4}$$

for a halfspace with viscosity η_1 (this decay constant is given by Bueler et al. (2007) equations 14 and 15). $\mathcal{R}$=$\mathcal{R}(\eta_2/\eta_1, h)$ is a function of the viscosity contrast η_2/η_1 between a viscous layer with thickness h and the halfspace below it:

$$\mathcal{R} = \frac{\begin{array}{r}2\tilde{\eta}\cosh(hk)\sinh(hk) + (1-\tilde{\eta}^2)h^2k^2 \\ + \tilde{\eta}^2\sinh^2(hk) + \cosh^2(hk)\end{array}}{\begin{array}{r}(\tilde{\eta}+\tilde{\eta}^{-1})\cosh(hk)\sinh(hk) + (\tilde{\eta}-\tilde{\eta}^{-1})hk \\ + \sinh^2(hk) + \cosh^2(hk)\end{array}}, \tag{5}$$

with $\tilde{\eta} = \eta_2/\eta_1$, used to compute model Best2 ($\tilde{\eta}_{\mathrm{Best2}} = 0.2$). For $\tilde{\eta} = 1$, $\mathcal{R} = 1$. The one-layer decay time constants for a uniform 10^{18} Pa s mantle are shown in Figure S1(a) (solid).

Following from the observation in Bueler et al. (2007) that, for a harmonic impulse (Heaviside) load $\hat{L}$, their model

*Current address, Climate and Space Research Bldg, 2455 Hayward Street, Ann Arbor, MI 48109 USA

0094-8276/20/$5.00

results in a deformation (integrating their equation 12)

$$\hat{U}(t) = \hat{L}T(1 - e^{-t/\tau}) \tag{6}$$

we can make a connection to the dynamics of a Maxwell-viscoelastic material. The relaxation of a Maxwell-viscoelastic body can be written as the sum of a set of independently relaxing exponential modes, called the Viscoelastic Normal Modes (Yuen & Peltier, 1982). The specific number of modes depends on the structure of the Earth model (Wolf, 1985), with more layers resulting in more modes. As with the viscous model above, the response of this material to the sudden imposition of a constant, harmonic load $\hat{L}$ (a Heaviside load) is (Vermeersen & Sabadini, 1997)

$$\hat{U}(t) = \hat{L}\sum_{i=1}^{m} T^i(1 - e^{-t/\tau^i}). \tag{7}$$

We can thus rewrite equation S1 to include these m modes by keeping track of each mode's independent deformation over time $\hat{U}^i$(t), discretized at times t_n, $\hat{U}^{i,n}$, and summing them:

$$\hat{U}^{n+1}_{\mathbf{k}} = \sum_{i=1}^{m} \frac{(\tau^i - \frac{1}{2}\Delta t)\hat{U}^{i,n}_{\mathbf{k}} + T^i\Delta t(\hat{L}^{n+1}_{\mathbf{k}})}{(\tau^i + \frac{1}{2}\Delta t)}, \tag{8}$$

where there is now a transfer function T^i and a decay constant τ^i associated with each mode.

1.1. GIA model coupling with BISICLES

To couple this model to BISICLES, which is a finite volume method, and thus written in terms of fluxes, we use a finite-difference approximation to the bedrock velocity to update the bedrock at each time-step of the ice evolution, including elastic deformation:

$$\dot{\hat{U}}^{n+1}_{\mathbf{k}} = \frac{\hat{U}^{n+1}_{\mathbf{k}} - \hat{U}^{n}_{\mathbf{k}}}{\Delta t} = T^{\mathrm{el}}\frac{\hat{L}^{n+1}_{\mathbf{k}} - \hat{L}^{n}_{\mathbf{k}}}{\Delta t} + \sum_{i=1}^{m}\frac{T^i\hat{L}^{n+1}_{\mathbf{k}} - \hat{U}^{i,n}_{\mathbf{k}}}{(\tau^i + \frac{1}{2}\Delta t)}. \tag{9}$$

This allows us to update the bedrock velocities at time intervals longer than the short timestep required to resolve the ice flow, except for the elastic component, which needs to be updated at every time step to maintain consistency. For these experiments, however, we coupled all GIA components at every timestep as the computational cost of the uplift calculation was minimal compared to the ice dynamic solver. The minimum timestep the BISICLES solver used was 0.015625 years (about 6 days).

1.2. Comparison with other GIA models

We can compare the deformation of a Maxwell-viscoelastic body with the viscous halfspace overlain by an elastic lithosphere by comparing the individual modes of deformation (Figure S1). For the Maxwell-viscoelastic body we use the analytical viscoelastic result from Wolf (1984) (2 viscoelastic modes and one elastic mode) and the modes computed by the spherically-symmetric, self-gravitating, incompressible calculator, TABOO (Spada, 2003). Though the stability of TABOO does not extend to the short wavelengths considered here (Spada, 2003), we can compare over a small area of overlap. The Bueler mode captures the dominant viscoelastic timescales of both models (Figure S1a) and where differences occur the magnitude of the mode's transfer function has diminished by orders of magnitude (Figure S1b). The computed fluid limit ($\sum_i T^i$, Figure S1c) is comparable for all the methods (TABOO uses a slightly different density in its layered model) and the elastic mode is slightly overestimated for wavelengths of interest (Figure S1d). The resulting difference in ice lost over the 150-year simulation never exceeds 1% in magnitude (Figure S1e).

2. Text S2. Committed Uplift

For the exponential mode model developed above, the uplift at time t due to a small harmonic ice mass loss dm (characterized by relaxation time τ) at time t' is

$$du = \frac{dm}{\rho_r}(\rho_r g T)\left(1 - \exp^{-(t-t')/\tau}\right). \tag{10}$$

For constant thinning starting at $t = 0$ with velocity v ($v > 0$), $dm = \rho_i v dt'$, the uplift is

$$u = \int_0^t \frac{\rho_i}{\rho_r}(\rho_r g T)v\left(1 - \exp^{-(t-t')/\tau}\right)dt'. \tag{11}$$

Integrated, this equals

$$u = \frac{\rho_i}{\rho_r}(\rho_r g T)v\left\{t + \tau\left(\exp^{-t/\tau} - 1\right)\right\}. \tag{12}$$

In equilibrium, the total uplift from the mass lost during this time ($\rho_i v t$) is $u_\infty = \rho_i g T v t$, thus the remaining uplift at time t if mass loss ceased, which we can call the committed uplift, is given by the expression

$$\Delta u = u_\infty - u = \frac{\rho_i}{\rho_r}(\rho_r g T)v\tau\left(1 - \exp^{-t/\tau}\right). \tag{13}$$

If this constant mass loss has been occurring for a time t much longer than the decay constant τ, then there is a steady state committed uplift of

$$\Delta u_{\mathrm{S.S.}} = u_\infty - u = (\rho_i g T)v\tau. \tag{14}$$

Though this assumption does not conserve mass or incorporate ice dynamics, it is an appropriate order-of-magnitude estimate, particularly for the small-wavelength loads whose decay constants τ are small (see figure 1b). It is apparent from expression 14 that the committed uplift becomes more important for higher-viscosity mantles (τ larger) and weaker lithospheres (larger T).

The committed uplift from 20 years of constant mass loss of 4 m/yr near the grounding line (Thomas et al., 2004; Rignot et al., 2014), is shown in figure S4. The steady-state surface uplift velocity from the loss only depends on the lithospheric rigidity, and is shown for three rigidities in figure S4(b-d). For the 25 km lithosphere of the UB model (10^{23} N m), the velocities are consistent with the observed uplift rates (Barletta et al., 2018), shown by the dots. For higher rigidities, the steady state velocities are smaller, and would need to be fit by modeling older (e.g., Last Glacial Maximum) losses more completely. The committed uplift from the grounding line mass loss is shown in figure S4(e-f) for viscosity models UB and Best2. The expected uplift is small ($\leq$ 1 m) for both models, and shows a broader area for the higher viscosity, higher rigidity model of Best2.

References

Barletta, V. R., Bevis, M., Smith, B. E., Wilson, T., Brown, A., Bordoni, A., ... Wiens, D. A. (2018). Observed rapid bedrock uplift in Amundsen Sea Embayment promotes ice-sheet stability. *Science*, *1339*(June), 1335–1339. doi: 10.1126/science.aao1447

Bueler, E., Lingle, C. S., & Kallen-Brown, J. a. (2007). Fast computation of a viscoelastic deformable Earth model for ice sheet simulation. *Ann. Glaciol.*, *46*, 97–105. doi: 10.3189/172756407782871567

Fretwell, P., Pritchard, H. D., Vaughan, D. G., Bamber, J. L., Barrand, N. E., Bell, R., ... Zirizzotti, A. (2013). Bedmap2: Improved ice bed, surface and thickness datasets for Antarctica. *Cryosphere*, *7*(1), 375–393. doi: 10.5194/tc-7-375-2013

Huybrechts, P. (2002, 1). Sea-level changes at the LGM from ice-dynamic reconstructions of the Greenland and Antarctic ice sheets during the glacial cycles. *Quaternary Science Reviews*, *21*(1-3), 203–231. Retrieved from http://linkinghub.elsevier.com/retrieve/pii/S0277379101000828 doi: 10.1016/S0277-3791(01)00082-8

Le Muir, E., & Huybrechts, P. (1996). A comparison of different ways of dealing with isostasy: examples from modelling the Antarctic ice sheet during the last glacial cycle. *Annals of glaciology*, *23*, 309–317. Retrieved from http://www.sciencedirect.com/science/article/pii/S0277379113003338%5Cnhttp://dx.doi.org/10.1038/ngeo411%5Cnhttp://www.sciencedirect.com/science/article/pii/B044452747800346X%5Cnhttps://sites.google.com/site/mnamaris/%5Cnhttp://adsabs.harvard.edu/abs/1959J doi: 10.1007/978-3-7091-0973-1{_}2

Nias, I. J., Cornford, S. L., & Payne, A. J. (2016). Contrasting the Modelled sensitivity of the Amundsen Sea Embayment ice streams. *Journal of Glaciology*, *62*(233), 552–562. doi: 10.1017/jog.2016.40

Rignot, E., Mouginot, J., Morlighem, M., Seroussi, H., & Scheuchl, B. (2014). Widespread, rapid grounding line retreat of Pine Island, Thwaites, Smith, and Kohler glaciers, West Antarctica, from 1992 to 2011. *Geophysical Research Letters*, *41*(10), 3502–3509. doi: 10.1002/2014GL060140

Spada, G. (2003). The theory behind TABOO. *Samizdat, Golden, Colo*.

Thomas, R., Rignot, E., Casassa, G., Kanagaratnam, P., Acuña, C., Akins, T., ... Zwally, J. (2004). Accelerated sea-level rise from west Antarctica. *Science*, *306*(5694), 255–258. doi: 10.1126/science.1099650

Vermeersen, L. L., & Sabadini, R. (1997). A new class of stratified viscoelastic models by analytical techniques. *Geophysical Journal International*, *129*(3), 531–570. doi: 10.1111/j.1365-246X.1997.tb04492.x

Wolf, D. (1984). The relaxation of spherical and flat Maxwell Earth models and effects due to the presence of the lithosphere. *Journal of Geophysics*, *56*(1), 24–33.

Wolf, D. (1985). The normal modes of a layered, incompressible Maxwell half-space. *Journal of Geophysics - Zeitschrift fur Geophysik*, *57*(2), 106–117.

Yuen, D. a., & Peltier, W. R. (1982). Normal modes of the viscoelastic earth. *Geophys. J. R. astr. Soc.*, *69*, 495526. doi: 10.1111/j.1365-246X.1982.tb04962.x

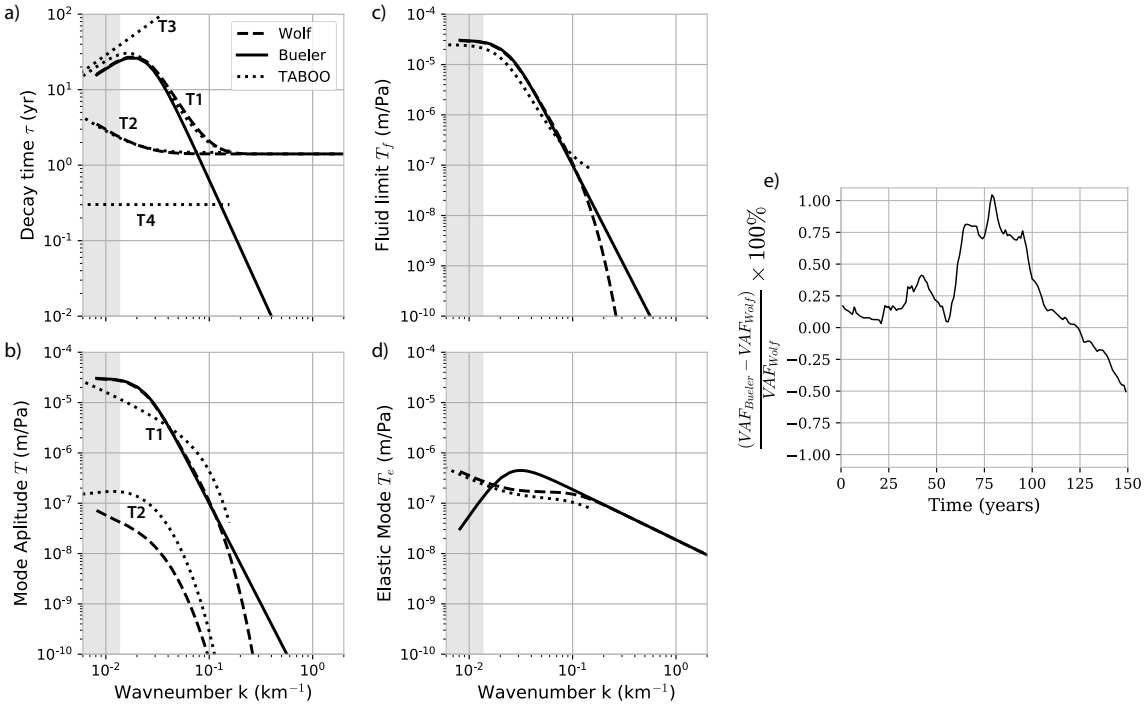

Figure S1. Comparison of mode decay times (a) and amplitudes (b-d) for a uniform mantle with viscosity 10^{18} Pa s overlain by a 25 km elastic lithosphere, computed using the two-mode Bueler viscous method (Bueler et al., 2007) (solid), the three-mode Wolf viscoelastic method (Wolf, 1984) (dashed), and a five mode model from the spherical, self-gravitating TABOO viscoelastic method (Spada, 2003) (dotted). Comparing the dominant viscoelastic modes (T1 in a,b), the decay times are very similar over the wavenumbers where the mode's amplitude is non-negligible (10^{-2} to 10^{-1} km^{-1}). Shaded regions show wavelengths larger than our computational domain. The amplitude of the T1 modes from the flat-earth models agree in this range. The second mode, T2, is significantly smaller in amplitude (b, by about three orders of magnitude). The third and fourth viscoelastic modes computed by TABOO (T3 and T4) have zero amplitude in this domain. c) The fluid (equilibrium) limit. d) The purely elastic mode. e) The difference over time in Volume Above Flotation (VAF) for coupled ice-dynamics simulation using the Bueler modes and Wolf modes.

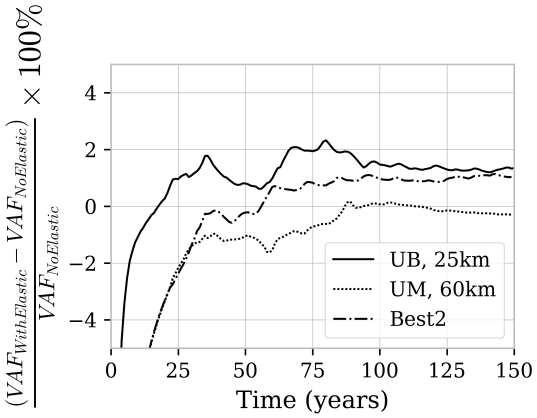

Figure S2. The percentage difference in total volume lost over time between coupling to GIA-related deformation including (equation 6) and omitting (equation 2) elastic uplift compared for rheological models UB (solid), "Best2" (dash-dot), and UM (dotted). The elastic component results in a large early difference that has mostly disappeared by 25 years in all models. The additional stability from including the elastic component beyond this is never more than 2%, demonstrating that its effect on mass loss is smaller than that due to viscoelastic deformation.

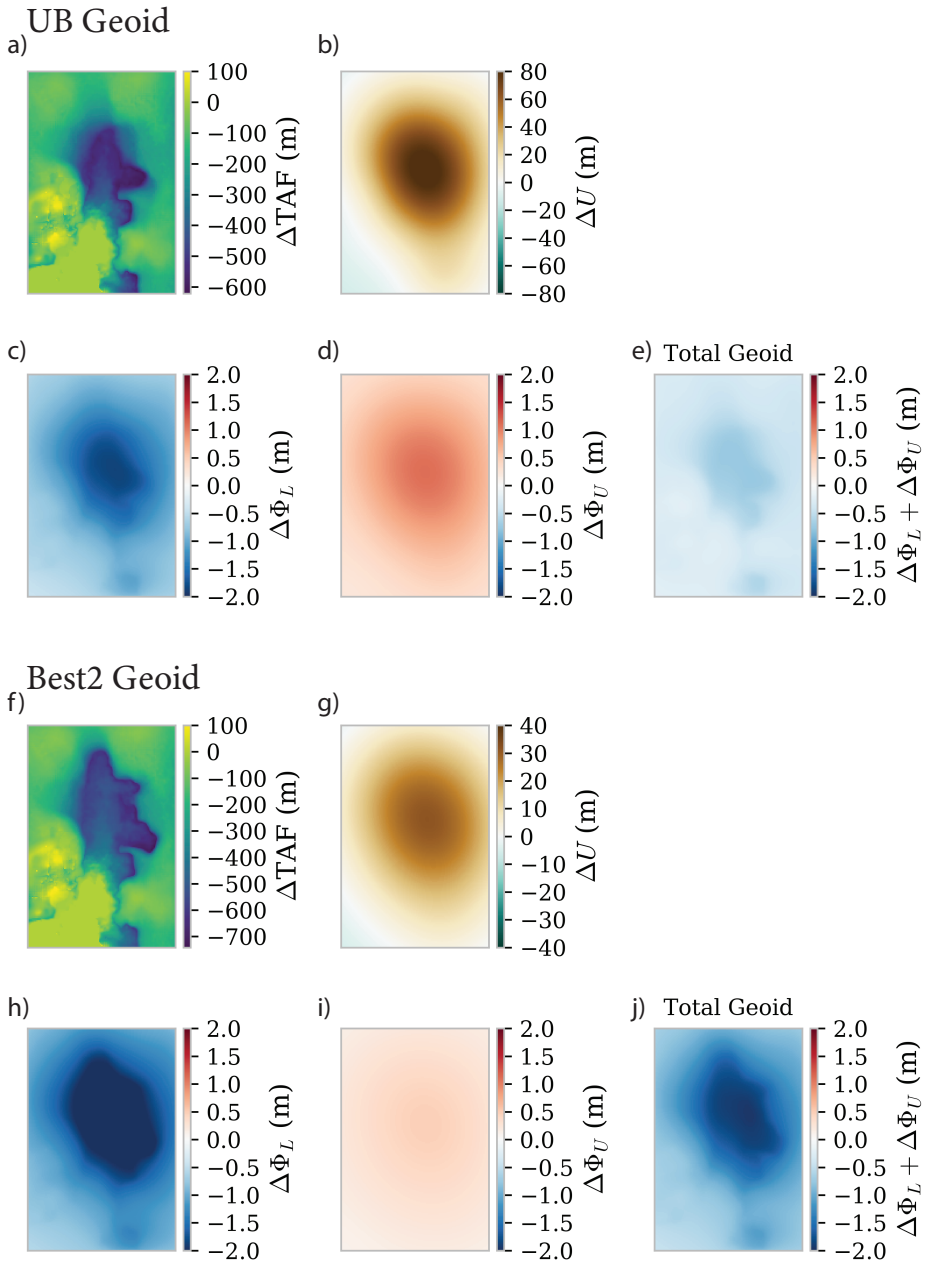

Figure S3. Estimate of the effect of the geoid perturbation to sea level compared to the uplift signal for the UB (a-e) and Best2 (f-j) models. The change in thickness above flotation from $t = 0$ to 150 years ΔTAF (a,f) and the change in bedrock over the same period ΔU (b, g) are shown along with their respective changes in geoid: $\Delta\Phi_L$ (c, h) and $\Delta\Phi_U$ (d, i). The sum of these components is the total change in geoid computed using equation 8 in the text (e,j) and is approximately the effect that the perturbations to the geoid have on local sea level. Comparing these with the effect on sea level from bedrock uplift (the negative of b, g) we see that the sea level effect of the geoid is smaller for both models: 2% for UB (25 km) to almost 6% for Best2.

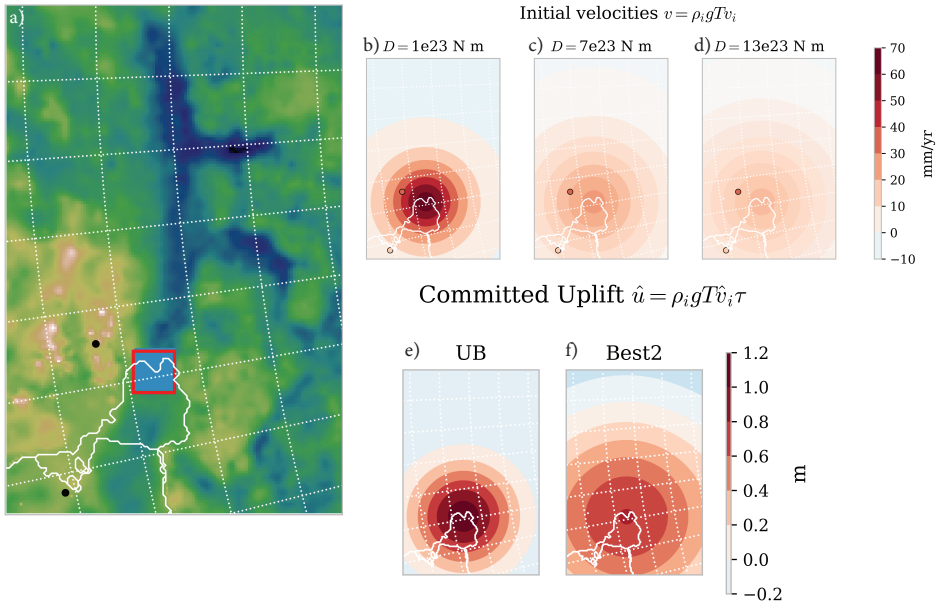

Figure S4. Committed uplift from recent mass loss. a) The blue box shows a 31 km box experiencing 4 m/yr thickness loss in the proximity of the grounding line over the Bedmap2 bathymetry (Fretwell et al., 2013). Black dots show nearby GPS observation locations (Barletta et al., 2018). b-d) Initial steady-state bedrock velocities assuming this ice-mass loss has occurred indefinitely given different lithosphere thicknesses: b) 25 km; c) 40 km; d) 60 km, with nearby GPS data (Barletta et al., 2018) shown in circles on the same color scale. e-f) The resulting committed uplift from this loss for viscosity model e) UB (25 km), and f) Best2.

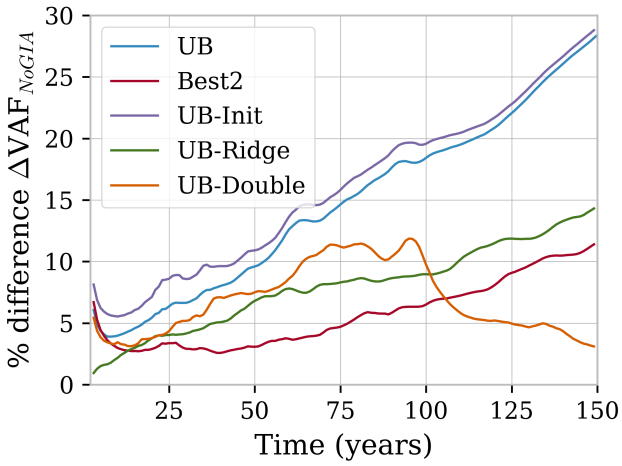

Figure S5. Additional simulations of the percentage difference in cumulative mass loss for ice dynamics coupled with viscoelastic uplift alone (with no pure elastic component) to the simulation with static bedrock (NoGIA). UB and Best2 are as in figure 2. UB-Init includes the initialized velocity from steady-state committed uplift (Figure S4), UB-Ridge uses the modified bedrock from Nias et al. (2016) with a decreased ridge in front of Pine Island Glacier, and UB-double doubles the basal melt rate. Note that the grounding line in the doubled melt rate simulation (UB-Double) reaches the edge of the domain at close to 100 years, resulting in the decrease in difference between the models (as the domain is emptied out).